

## $\text{Cu}_2\text{S}/\text{Ni}_x\text{S}_y$ multi-interfaces induced Ni (III) for optimizing alkaline hydrogen evolution reaction

Fei Yuan,<sup>\*a</sup> Xiaoteng Wang,<sup>a</sup> Gang Liu<sup>a</sup> and Yang Liu<sup>a</sup>

*<sup>a</sup>College of Chemistry and Chemical Engineering, Northwest Normal University, Lanzhou, Gansu 730070, China.*

*E-mail: yuanf@nwnu.edu.cn*

### **Experiment section**

#### **Materials and chemicals**

Nickel (II) chloride hexahydrate puratre ( $\text{NiCl}_2 \cdot 6\text{H}_2\text{O}$ ,  $\geq 98\%$ ) was purchased from Beijing Hongxing Co. Ltd. Copper chloride ( $\text{CuCl}_2 \cdot 2\text{H}_2\text{O}$ ,  $\geq 99\%$ ) was got from Tianjin Guangfu technology Co. Ltd. Ethylene glycol ( $\text{C}_2\text{H}_6\text{O}_2$ , EG,  $\geq 99.5\%$ ) was gained from Tianjin Medical Chemistry Co. Ltd. Hydrazine hydrate ( $\text{N}_2\text{H}_4 \cdot \text{H}_2\text{O}$ ,  $\geq 80\%$ ) was obtained from Tianjin Damao technology Co. Ltd. S powder (S,  $\geq 98\%$ ) was gained from Tianjin Guangfu technology Co. Ltd. Pt/C (20 wt%) and Nafion (5 wt%) were supplied by Alfa Aesar. In addition, all of reagents used in this experiment were analytically pure without purification.

#### **Characterization**

The powder X-ray diffraction (XRD) were conducted by using Cu-K $\alpha$  radiation as the X-ray source in the  $2\theta$  range of  $20^\circ$  -  $80^\circ$ . X-ray photoelectron spectroscopy (XPS) was performed using a Kratos AXIS Ultra DLD instruments with a monochromatic X-ray source (AL K $\alpha$   $h\nu$  =

1486.6) and all elemental peaks were revised by the standard position of C 1s peak. Transmission electron microscope (TEM) images were observed with a Tecnai<sup>TM</sup> G<sup>2</sup>F30, FEI operating at 200 KV, equipped with energy dispersive X-ray spectroscopy (EDX, Tecnai G2, USA).

### **Electrochemical measurement**

Generally, 4 mg black catalyst powder was dissolved in a 1 mL solution which was composed of ethanol and ultrapure water in a 1:1 volume ratio. Then, 30  $\mu$ L Nafion aqueous solution (0.5 wt%) was added into the 1 mL solution mentioned earlier and ultrasonicated it for 0.5 h to form a uniform black solution. Eventually, 5  $\mu$ L black solution was drop on the 3.0 mm diameter glassy carbon electrode serving as the working electrode (loading 0.286 mg cm<sup>-2</sup>). In this article, all the electrochemical tests were realized through electrochemical workstation (CHI 660E, Shanghai Chenhua) with three-electrode configuration without *iR* compensation and at room temperature. In the test, a graphite carbon rod was utilized as contrast electrode, while the saturated Ag/AgCl electrode was treated as the reference electrode. All potentials (vs. Ag/AgCl) appearing in the article were transformed into reversible hydrogen electrode (RHE), which were corrected by means of using the Nernst equation:  $E \text{ (vs. RHE)} = E \text{ (vs. Ag/AgCl)} + 0.059 \text{ pH} + 0.198 \text{ V}$ .

### **HER measurement**

The HER electrochemical activities were all measured in 1.0 M KOH

electrolyte. Linear sweep voltammetry (LSV) polarization curves were investigated in the range of - 0.8 V - -1.8 V vs. Ag/AgCl with a scan rate of 5 mV s<sup>-1</sup>. The electrochemical impedance spectroscopy (EIS) measurements were tested at -120 mV vs. Ag/AgCl from 10<sup>5</sup> to 0.01 Hz. In order to obtain the electrochemically active surface areas of all the catalysts, cyclic voltammograms (CVs) were investigated between -0.8 V and -0.7 V with the different scan rates (20 - 200 mV s<sup>-1</sup>). In addition, the HER stability of the catalysts was also performed by Amperometric i-t Curve at -1.20 V vs. RHE for 33 h. All the current density of the catalysts were rectified to the geometrical surface area of the GCE (0.07cm<sup>2</sup>).

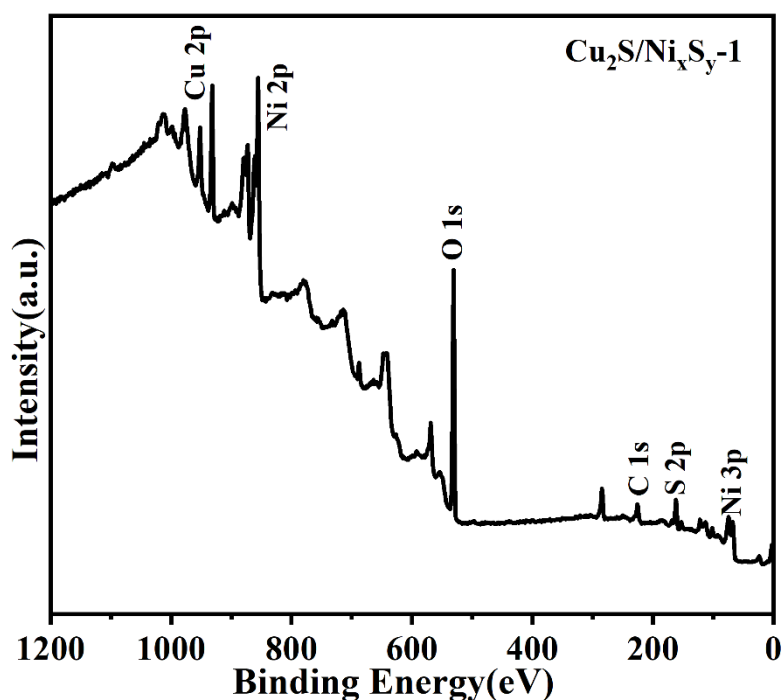


**Fig. S1.** The full XPS survey spectra of the Cu<sub>2</sub>S/Ni<sub>x</sub>S<sub>y</sub>-1.

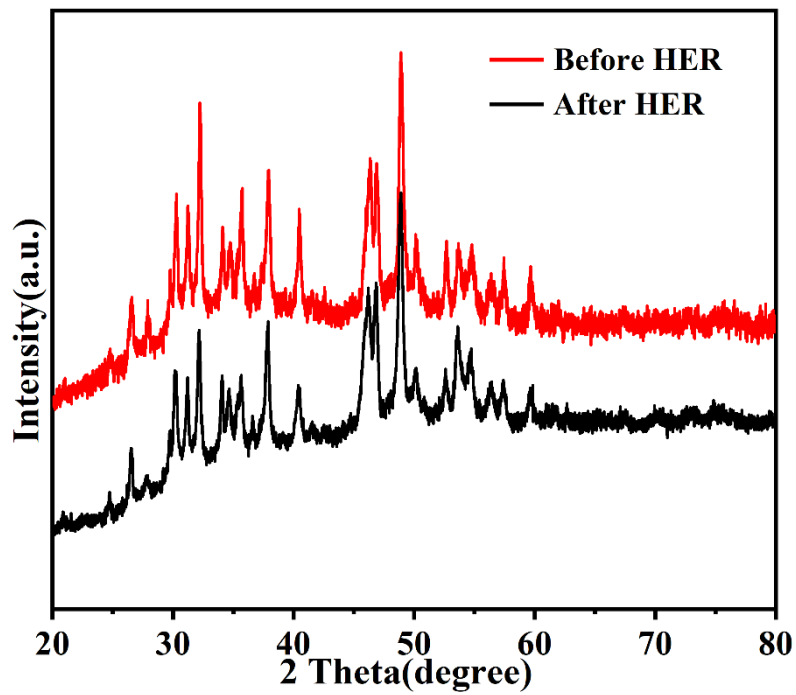


**Fig. S2.** XRD patterns of  $\text{Cu}_2\text{S}/\text{Ni}_x\text{S}_y\text{-1}$  after stability test.

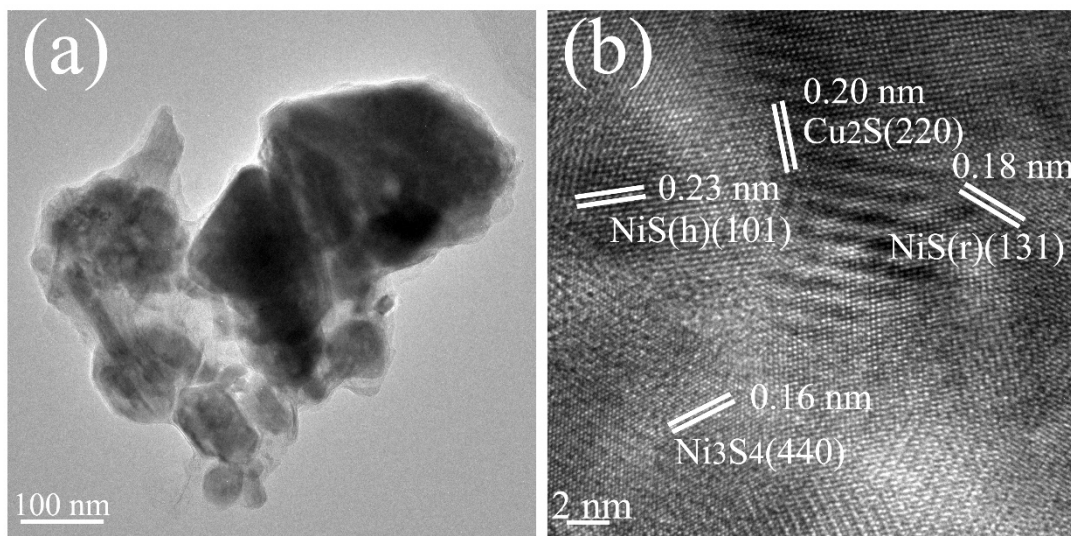


**Fig. S3.** The TEM and TRTEM of  $\text{Cu}_2\text{S}/\text{Ni}_x\text{S}_y\text{-1}$  after stability test.

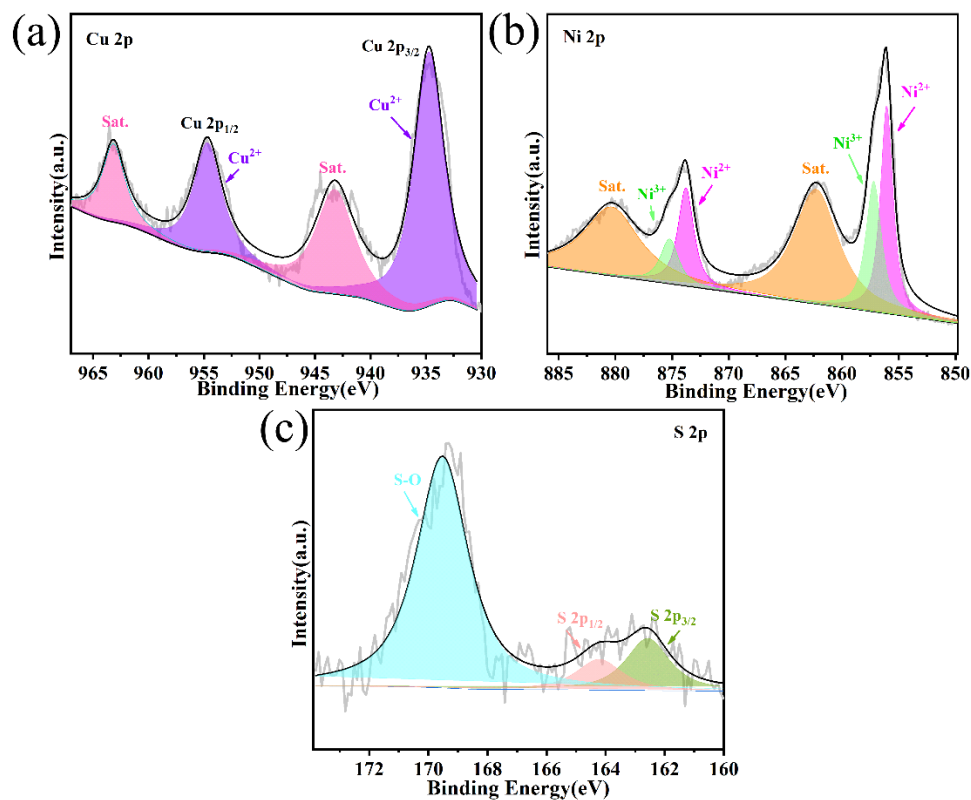


**Fig. S4.** (a) Cu 2p (b) Ni 2p (c) S 2p spectra of  $\text{Cu}_2\text{S}/\text{Ni}_x\text{S}_y-1$  after stability test.

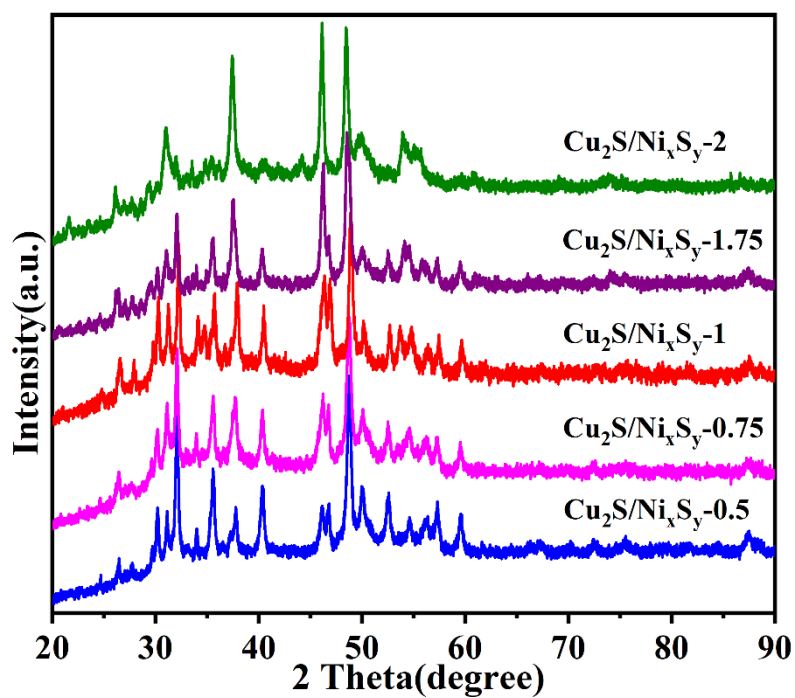


**Fig. S5.** XRD patterns of  $\text{Cu}_2\text{S}/\text{Ni}_x\text{S}_y-0.5$ ,  $\text{Cu}_2\text{S}/\text{Ni}_x\text{S}_y-0.75$ ,  $\text{Cu}_2\text{S}/\text{Ni}_x\text{S}_y-1$ ,  $\text{Cu}_2\text{S}/\text{Ni}_x\text{S}_y-1.75$  and  $\text{Cu}_2\text{S}/\text{Ni}_x\text{S}_y-2$ .

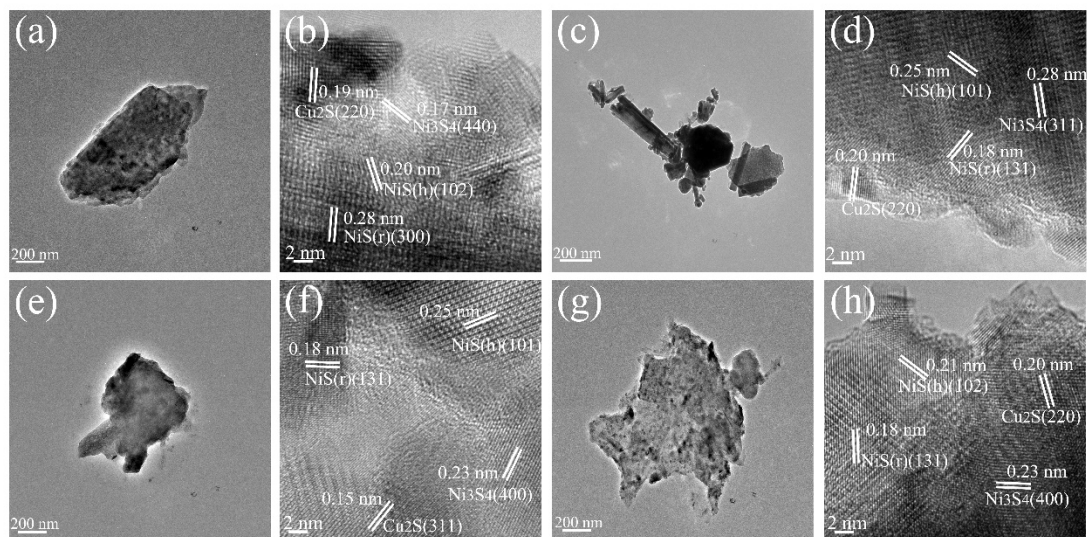


**Fig. S6.** TEM and TRTEM of (a, b)  $\text{Cu}_2\text{S}/\text{Ni}_x\text{S}_y\text{-0.5}$  (c, d)  $\text{Cu}_2\text{S}/\text{Ni}_x\text{S}_y\text{-0.75}$  (e, f)  $\text{Cu}_2\text{S}/\text{Ni}_x\text{S}_y\text{-1.75}$  and (g, h)  $\text{Cu}_2\text{S}/\text{Ni}_x\text{S}_y\text{-2}$ .

**Table S1.** Initial dosage mass (mmol) of raw stuff in the prepared  $\text{Cu}_2\text{S}/\text{Ni}_x\text{S}_y\text{-n}$  electrocatalysts.

Sample	0.5	0.75	1	1.75	2
$\text{Cu}_2\text{S}/\text{Ni}_x\text{S}_y\text{-n}$					
$\text{CuCl}_2 \cdot 2\text{H}_2\text{O}$	0.5	0.75	1	1.75	2
$\text{NiCl}_2 \cdot 6\text{H}_2\text{O}$	1	1	1	1	1
S	2	2	2	2	2

**Table S2.** Content of Cu, Ni and S in the  $\text{Cu}_2\text{S}/\text{Ni}_x\text{S}_y\text{-n}$  electrocatalysts estimated from ICP-OES measurements.

Sample	0.5	0.75	1	1.75	2
$\text{Cu}_2\text{S}/\text{Ni}_x\text{S}_y\text{-n}$					
Cu (wt.%)	30.62	43.13	50.71	43.15	45.19
Ni (wt.%)	45.48	38.50	32.38	25.95	25.99

S (wt.%)	2.81	2.69	2.66	2.58	2.19
Cu/Ni	0.67	1.12	1.56	1.66	1.74

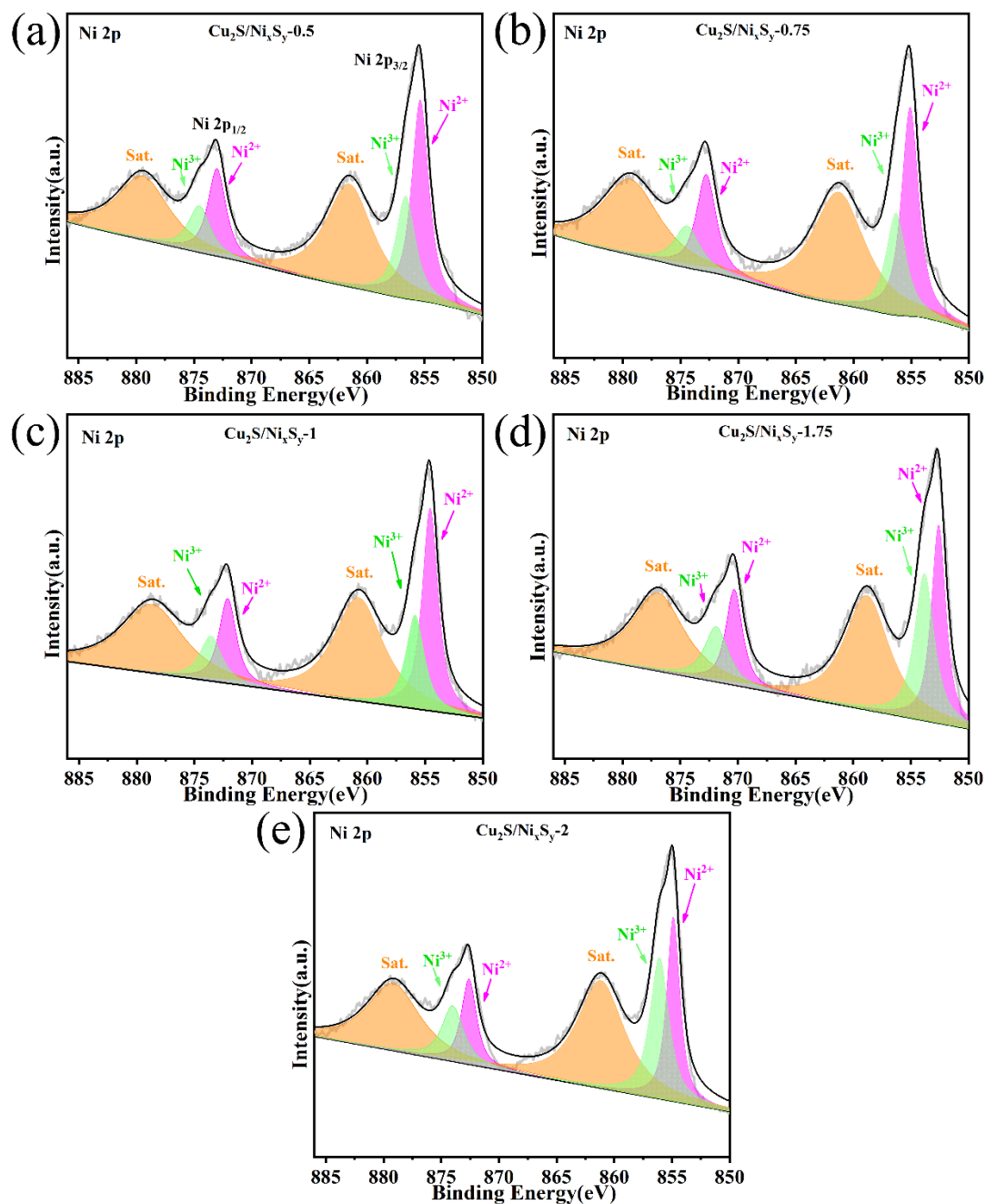


**Fig. S7.** Ni 2p XPS spectra of (a) Cu<sub>2</sub>S-Ni<sub>x</sub>S<sub>y</sub>-0.5 (b) Cu<sub>2</sub>S-Ni<sub>x</sub>S<sub>y</sub>-0.75 (c) Cu<sub>2</sub>S-Ni<sub>x</sub>S<sub>y</sub>-1 (d) Cu<sub>2</sub>S-Ni<sub>x</sub>S<sub>y</sub>-1.75 (e) Cu<sub>2</sub>S-Ni<sub>x</sub>S<sub>y</sub>-2.

**Table S3.** The properties of the as-prepared electrocatalysts

Sample	0.5	0.75	1	1.75	2
Cu <sub>2</sub> S/Ni <sub>x</sub> S <sub>y</sub> -n					
Ni <sup>3+</sup> (wt.%)	19.13	16.76	20.01	24.16	23.98

The Ni<sub>3</sub>S<sub>4</sub>, NiS (r) and NiS (h) of the samples were quantitatively analyzed by XRD peak intensity comparison. In Fig. 1a, according to the standard XRD diffraction peaks of Ni<sub>3</sub>S<sub>4</sub> (JCPDS Card No. 76-1813), NiS (r) (JCPDS Card No. 12-41) and NiS (h) (JCPDS Card No. 65-830), we can see that the peaks corresponding to (311), (300) and (220) are diffraction peaks with strong relative intensity of Ni<sub>3</sub>S<sub>4</sub>, NiS (r) and NiS (h), respectively. The specific strength and ratio are shown in the Table S1.

**Table S4.** The intensity of XRD peaks (cm) corresponding to Ni<sub>3</sub>S<sub>4</sub>, NiS (r) and NiS (h), and the proportion of Ni<sub>3</sub>S<sub>4</sub> in the total Ni.

Sample	0.5	0.75	1	1.75	2
Cu <sub>2</sub> S/Ni <sub>x</sub> S <sub>y</sub> -n					
Ni <sub>3</sub> S <sub>4</sub> (311)	0.69	0.88	0.81	0.67	0.91
NiS (r) (300)	1.89	1.49	1.64	1.07	0.44
NiS (h) (220)	0.66	0.93	1.20	1.55	2.13
sum	3.24	3.30	3.65	3.31	3.48
Ni <sub>3</sub> S <sub>4</sub> (wt.%)	21.29	26.66	22.19	20.24	26.14



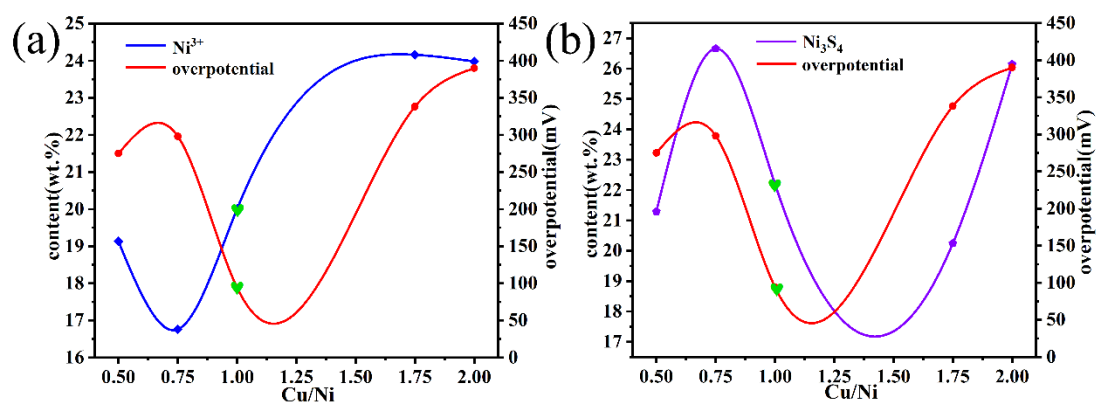


**Fig. S8.** (a) relationship between  $\text{Ni}^{3+}$  and overpotential at different ratios of Cu and Ni (b) relationship between  $\text{Ni}_3\text{S}_4$  and overpotential at different ratios of Cu and Ni.

**Table S5.** Comparison of the nickel sulfide compound catalysts HER activity in alkaline electrolyte.

catalyst	Tafel slope (mV dec <sup>-1</sup> )	Overpotential (mV)	Ref.
Ni/NiS/P, N, S– rGO	135.00	155	1
Zn–NiS-3	113.00	208	2
NiS@C	89.00	232	3
NiS film	143.30	290	4
$\text{Ni}_3\text{S}_2$ @NiS- 250/NF	75.50	129	5
NiS/VS	116.10	158	6
Ni-M@C-130	50.80	123	7
NiS film	125.00	169	8

Cu <sub>2</sub> S/Ni <sub>x</sub> S <sub>y</sub> -1	97.69	94	This work
1.	M. B. Z. Hegazy, M. R. Berber, Y. Yamauchi, A. Pakdel, R. Cao and U.-P. Apfel, Synergistic Electrocatalytic Hydrogen Evolution in Ni/NiS Nanoparticles Wrapped in Multi-Heteroatom-Doped Reduced Graphene Oxide Nanosheets, <i>ACS Applied Materials &amp; Interfaces</i> , 2021, <b>13</b> , 34043-34052.		
2.	C. Prakash, P. Sahoo, R. Yadav, A. Pandey, V. K. Singh and A. Dixit, Nanoengineered Zn-Modified Nickel Sulfide (NiS) as a Bifunctional Electrocatalyst for Overall Water Splitting, <i>International Journal of Hydrogen Energy</i> , 2023, <b>48</b> , 21969-21980.		
3.	J. Zhang, Y. Wang, J. Cui, J. Wu, X. Shu, C. Yu, H. Bai, M. Zhai, Y. Qin, H. Zheng, Y. Zhu, Y. Zhang and Y. Wu, In-Situ Synthesis of Carbon-Coated $\beta$ -NiS Nanocrystals for Hydrogen Evolution Reaction in Both Acidic and Alkaline Solution, <i>International Journal of Hydrogen Energy</i> , 2018, <b>43</b> , 16061-16067.		
4.	G. Rahman, S. Y. Chae and O.-s. Joo, Efficient Hydrogen Evolution Performance of Phase-pure NiS Electrocatalysts Grown on Fluorine-Doped Tin Oxide-Coated Glass by Facile Chemical Bath Deposition, <i>International Journal of Hydrogen Energy</i> , 2018, <b>43</b> , 13022-13031.		
5.	M. Chen, Q. Su, N. Kitiphatpiboon, J. Zhang, C. Feng, S. Li, Q. Zhao, A. Abudula, Y. Ma and G. Guan, Heterojunction Engineering of		

Ni<sub>3</sub>S<sub>2</sub>/NiS Nanowire for Electrochemical Hydrogen Evolution, *Fuel*, 2023, **331**, 125794.

6. K. Bao, Y. Yan, T. Liu, T. Xu, J. Cao and J. Qi, Constructing NiS–VS Heterostructured Nanosheets for Efficient Overall Water Splitting, *Inorganic Chemistry Frontiers*, 2020, **7**, 4924-4929.
7. K. Srinivas, Y. Chen, X. Wang, B. Wang, M. Karpuraranjith, W. Wang, Z. Su, W. Zhang and D. Yang, Constructing Ni/NiS Heteronanoparticle-Embedded Metal–Organic Framework-Derived Nanosheets for Enhanced Water-Splitting Catalysis, *ACS Sustainable Chemistry & Engineering*, 2021, **9**, 1920-1931.
8. G. Kalaiyarasan, K. Aswathi and J. Joseph, Formation of Nanoporous NiS Films from Electrochemically Modified GC Surface with Nickel Hexacyanoferrate Film and its Performance for the Hydrogen Evolution Reaction, *International Journal of Hydrogen Energy*, 2017, **42**, 22866-22876.